Magnetoexcitons and Faraday rotation in single-walled carbon nanotubes and graphene nanoribbons

Jonas Have[1,2,*] and Thomas G. Pedersen[1,3]

[1]*Department of Materials and Production, Aalborg University, DK-9220 Aalborg East, Denmark*
[2]*Department of Mathematical Sciences, Aalborg University, DK-9220 Aalborg East, Denmark*
[3]*Center for Nanostructured Graphene (CNG), DK-9220 Aalborg East, Denmark*

The magneto-optical response of single-walled carbon nanotubes (CNTs) and graphene nanoribbons (GNRs) is studied theoretically, including excitonic effects. Both diagonal and nondiagonal response functions are obtained and employed to compute Faraday rotation spectra. For single-walled CNTs in a parallel field, the results show field-dependent splitting of the exciton absorption peaks caused by brightening a dark exciton state. Similarly, for GNRs in a perpendicular magnetic field, we observe a field-dependent shift of the exciton peaks and the emergence of an absorption peak above the energy gap. Results show that excitonic effects play a significant role in the optical response of both materials, particularly for the off-diagonal tensor elements.

I. INTRODUCTION

Single-walled carbon nanotubes (CNTs) and graphene nanoribbons (GNRs) are prominent quasi-one-dimensional carbon-based structures defined geometrically as cylindrical tubes and thin strips of graphene, respectively. The two materials are intimately related, since GNRs can be regarded as (and produced from) unrolled CNTs [1,2]. Moreover, both materials have a large number of potential applications in various areas of electronics and optoelectronics [3–6]. The reduced dimensionality and screening of narrow GNRs and small radius CNTs lead to excitons with binding energy on the order of a few hundred meV [7–10]. Therefore, excitons have a strong impact on the optical response of both CNTs [9] and GNRs [11,12] and must be accounted for in models of the optical response.

Excitons are sensitive to a number of external perturbations, such as electric and magnetic fields. For instance, magnetic fields can be used as an effective tool to probe various properties of excitons, including their transport [13] and spatial extent [14]. Additionally, an accurate understanding of the dynamics of magnetoexcitons reveals details of the role played by magnetic fields in optoelectronic devices [15,16]. The electronic and optical properties of CNTs in the presence of a static magnetic field were considered theoretically in a series of papers by Ando [17–19], and the results were later verified experimentally [20–26]. However, the off-diagonal elements of the conductivity tensor were not evaluated in these papers. The presence of an external magnetic field breaks time-reversal symmetry and results in finite off-diagonal conductivity elements [27], also called the Hall conductivities. Calculating the off-diagonal conductivity for CNTs and GNRs is one of the objectives in the present paper. The Hall conductivity gives rise to the optical Hall effect manifesting itself as Faraday

rotation [28] of the electromagnetic field, which is important for several electro-optic applications [29,30]. The Faraday rotation for CNTs [28] and GNRs [31] has been calculated in the independent-particle approximation. But, as discussed above, this approximation is not well suited to describe the optical response of CNTs and GNRs. The solution is to include excitonic effects, which we do in the present work.

With respect to GNRs, the amount of theoretical work is rather limited compared to the case of CNTs. The available works either focus on GNRs in the presence of a magnetic field without excitons [32,33] or the converse [11,12] (i.e., including excitons but not an external magnetic field). In the present work, we improve upon this by calculating the magnetoexcitonic response for a range of GNRs.

An additional interesting aspect of quasi-one-dimensional systems, including CNTs, GNRs, and conjugated polymers, is that these can serve as convenient test systems for theoretical methods. Recent years have seen an increase in experimental work on magnetoexcitonic effects in two-dimensional semiconductors such as transition metal dichalcogenides [34–37]. In this class of materials, a number of challenges limit theoretical models of magnetoexcitons to effective-mass models [38]. In comparison, quasi-one-dimensional systems are much less computationally demanding. As a consequence, it is possible to obtain an accurate description of magnetoexcitons in these systems. Thus, we will present calculations of all the elements of the linear optical conductivity tensor for a number of different CNTs and GNRs. Our calculations are based on a tight-binding model that provides the independent-particle properties, while the excitonic properties are obtained from the Bethe-Salpeter equation.

II. THEORETICAL MODELS

In this section, we will briefly describe the applied theoretical models and computational tools. The GNR and CNT structures are illustrated in Fig. 1. In general, both GNRs
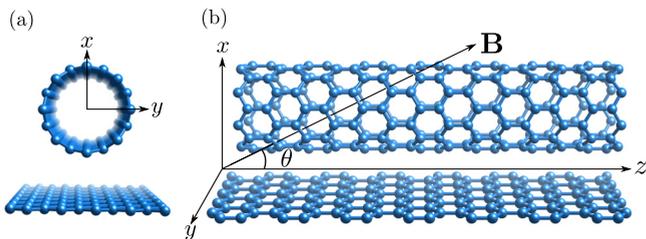
*jh@nano.aau.dk

FIG. 1. (a) CNT and GNR structures as seen in the direction of the z axis. (b) Side view of the CNT and GNR structures. The GNR structure is parallel to the yz plane, with a magnetic field at an angle θ to the yz plane and in the xz plane.

and CNTs exist in a variety of geometries. Hence, GNRs are characterized by their width and edge type, whereas CNTs are defined by their chiral index (n, m) that, in turn, determines diameter and chirality [39]. However, in the present work, we limit ourselves to zigzag CNTs with chiral indices $(n, 0)$ for $n \in \mathbb{N}_+$, and armchair GNRs characterized by the number of dimer lines N across the ribbon, which we denote by N-AGNRs. We ignore any effects of geometrical relaxation of edge atoms. For calculation of the independent-particle energies and wave functions, we apply a nonorthogonal π-electron nearest-neighbor tight-binding (TB) model. Studies have shown that the single-particle properties of carbon-based materials, e.g., graphene, CNTs, and GNRs, are well described by π-electron TB models [39,40]. The choice of a nonorthogonal (in contrast to the usual orthogonal) TB model is made to break the electron-hole symmetry, as electron-hole symmetry results in Hall conductivities that are identically zero [27,28].

The external magnetic field is introduced via the minimal substitution of the momentum operator $\hat{\mathbf{p}} \mapsto \hat{\boldsymbol{\pi}} = \hat{\mathbf{p}} + e\mathbf{A}$, where $\mathbf{A}$ denotes the magnetic vector potential, related to the magnetic field $\mathbf{B}$ via $\mathbf{B} = \nabla \times \mathbf{A}$. In a TB model, the substitution gives rise to a Peierls phase factor in the hopping integrals t such that $t \mapsto t_{ij} = t e^{i\phi_{ij}}$, with the Peierls phase given by [41]

$$\phi_{ij} = \frac{e}{\hbar} \int_{\mathbf{R}_i}^{\mathbf{R}_j} \mathbf{A} \cdot d\mathbf{l}, \qquad (1)$$

where $\mathbf{R}_i$ and $\mathbf{R}_j$ denote the location of atoms at site i and j, respectively. For periodic systems in more than one dimension, the phase factor necessarily breaks the translation symmetry. However, given an appropriate choice of gauge, the translation symmetry can be preserved in one-dimensional (1D) systems. This fact is responsible for the relative tractability of 1D magnetoexcitons, in contrast to two and three dimensions (2D, 3D). The appropriate gauge depends on the direction of the magnetic field. As illustrated in Fig. 1, we take the long axis along z and consider a magnetic field $\mathbf{B} = B(\sin\theta \hat{\mathbf{x}} + \cos\theta \hat{\mathbf{z}})$, where θ is the angle between field and long axis, and $B = |\mathbf{B}|$ is the magnetic field strength. For this geometry, the symmetry-preserving gauge is

$$\mathbf{A} = -By(\cos\theta \hat{\mathbf{x}} - \sin\theta \hat{\mathbf{z}}). \qquad (2)$$

Below, however, we only consider parallel ($\theta = 0$) and perpendicular ($\theta = \pi/2$) magnetic fields. Moreover, for GNRs we only consider perpendicular fields, since the electronic

structure and optical response of GNRs are unaffected by a parallel field.

A. Excited states

Using the independent-particle energies and wave functions, the exciton states of the systems can be found by solving the Bethe-Salpeter equation (BSE) [7,42,43]. The excited states $|\text{exc}\rangle$ can be expanded as

$$|\text{exc}\rangle = \sum_{cvk} \Psi_{cvk} |vk \rightarrow ck\rangle, \qquad (3)$$

where Ψ_{cvk} are the expansion coefficients, and $|vk \rightarrow ck\rangle$ are the singlets of singly excited states between the valence (v) and conduction (c) bands at k. Using the expansion of the excited states in Eq. (3), the BSE is expressed as

$$E_{cvk} \Psi_{cvk} + \sum_{c'v'k'} K_{cvk,c'v'k'} \Psi_{c'v'k'} = E_{\text{exc}} \Psi_{cvk}, \qquad (4)$$

$$K_{cvk,c'v'k'} := W_{cvk,c'v'k'} - 2V_{cvk,c'v'k'},$$

where E_{exc} is the exciton energy, $E_{cvk} = E_{ck} - E_{vk}$, $V_{cvk,c'v'k'}$ is the exchange matrix element, and $W_{cvk,c'v'k'}$ is the Coulomb interaction matrix element. We follow Ref. [44] and calculate the exchange and Coulomb interaction matrix elements using an Ohno-type potential, which has been shown to produce results that compare well with more advanced models and experiments for quasi-1D systems [44]. In this approximation, the bare electron-hole interaction takes the form

$$v(\mathbf{r}_e - \mathbf{r}_h) = -U \left[1 + \left(\frac{4\pi\epsilon_0 U}{e^2} \right)^2 |\mathbf{r}_e - \mathbf{r}_h|^2 \right]^{-\frac{1}{2}}, \qquad (5)$$

where $\mathbf{r}_e$ and $\mathbf{r}_h$ are the position of the electron and hole, respectively, and $U = 11.3$ eV is the Hubbard energy [45]. The screened Coulomb interaction matrix elements are then calculated using $W(\mathbf{r}_e - \mathbf{r}_h) = v(\mathbf{r}_e - \mathbf{r}_h)/\epsilon$, where ϵ is the screening parameter. The Coulomb term is screened by both the self-screening and the screening from the surrounding media. Similarly, the exchange matrix elements can be calculated using $W(\mathbf{r}_e - \mathbf{r}_h) = v(\mathbf{r}_e - \mathbf{r}_h)/\epsilon_{exc}$, where ϵ_{exc} denotes the screening of the exchange term. According to Ref. [46], the exchange term should only be screened by the surrounding media; thus we have that $\epsilon_{exc} < \epsilon$.

It is worth noting that the dimension of the eigenvalue problem in Eq. (4) is given by $N_c \times N_v \times N_k$, where N_c, N_v, and N_k are the number of conduction bands, valence bands, and k points, respectively. Even for a reasonably small system such as the (8,0) CNT, which has 32 atoms in the unit cell and a k grid with 150 points, the Bethe-Salpeter matrix (BSM) has dimension $38\,400 \times 38\,400$. Thus, using this method for typical chiral CNTs such as (6,5) CNTs with unit cells containing several hundred atoms is computationally unfeasible.

B. Optical response

The evaluation of the optical conductivity tensor, in the presence of electron-hole interactions, follows that of Ref. [47]. The many-body momentum operator acting on the many-body

ground state is

$$|P_i\rangle := \hat{P}_i|0\rangle = \sqrt{2} \sum_{cvk} p_{cvk}^i \Psi_{cvk}, \qquad (6)$$

where $|0\rangle$ is the many-body ground state and $\hat{P}_i$ and p_{cvk}^i are the many-body momentum operator and the single-particle momentum matrix elements in direction $i \in \{x,y,z\}$, respectively. Ignoring the nonresonant terms of the optical conductivity tensor, the real part of the tensor elements can be expressed as [47]

$$\mathrm{Re}\,\sigma_{ij} = -\frac{e^2}{m^2\omega A} \mathrm{Im}\langle P_i|\hat{G}(\hbar\omega)|P_j\rangle, \qquad (7)$$

where $\hbar\omega$ is the photon energy, $\hat{G}(\hbar\omega)$ is the many-body Green's function, and A is the cross-sectional area of the system, where the height of the ribbon and the wall thickness of the tubes is taken to be $d = 3.35$ Å [48]. In terms of the many-body Hamiltonian $\hat{H}$, the Green's function $\hat{G}(\hbar\omega)$ is defined by

$$\hat{G}(\hbar\omega) := \lim_{\eta\to 0^+} \frac{1}{\hbar\omega - \hat{H} + i\eta}. \qquad (8)$$

To increase the numerical stability, we use a finite $\eta \approx 1$ meV in Eq. (8), and to add additional broadening to the spectra obtained by Eq. (7), we convolute with a Lorentzian line-shape function having a width Γ.

The off-diagonal tensor elements, i.e., σ_{ij} for $i \neq j$, are the so-called Hall conductivities. This notation stems from the fact that, if the off-diagonal tensor elements are finite, the system exhibits the optical Hall effect, in analogy to the electric Hall effect in the static case. The optical Hall effect is closely related to the Faraday rotation of a material [27,28], whereby the polarization plane of light rotates as the wave propagates in the material under the influence of a magnetic field. The Faraday rotation for a weak magnetic field in the z direction reads [27]

$$\phi = \frac{l}{2c\epsilon_0} \frac{n\,\mathrm{Re}\,\sigma_{xy} - \kappa\,\mathrm{Im}\,\sigma_{xy}}{n^2 + \kappa^2} \rho, \qquad (9)$$

where l is the propagation distance of the light, c is the speed of light, ϵ_0 is the vacuum permittivity, ρ is an effective volume fraction of either AGNRs or CNTs in space, and $n + i\kappa$ is the complex refractive index at $B = 0$. In the idealized situation, where either CNTs or AGNRs are packed tightly in space, the volume fraction is $\rho = 1$ and otherwise $0 \leqslant \rho < 1$. For weak magnetic fields the Hall conductivities are linear in B [27], and the Faraday rotation can be expressed $\phi = VlB\rho$, where V is the Verdet constant. Measurements of the Faraday rotation provide a convenient experimental method for determining the optical Hall conductivity, even at low magnetic field strengths [49].

With regards to the diagonalization of the BSM, a significant reduction in computation time can be obtained if one does not need the eigenvalues and eigenstates of the BSE but only the matrix elements of the Green's function, which can be calculated effectively using the Lanczos-Haydock routine [50]. The routine allows for efficient evaluation of matrix elements of the type $\langle u|\hat{G}|u\rangle$ by a recursive tridiagonalization of the Hamiltonian and subsequent evaluation of the matrix element

using continued fractions. When convergence of the continued fractions is obtained, the calculations can be truncated. For evaluation of the Hall conductivities involving off-diagonal matrix elements of the type $\langle v|\hat{G}|u\rangle$, one can make use of the relation

$$\langle v + iu|\hat{G}|v + iu\rangle = \langle v|\hat{G}|v\rangle + \langle u|\hat{G}|u\rangle + i2\mathrm{Im}\langle v|\hat{G}|u\rangle \qquad (10)$$

and the similar relation for $\langle v + u|\hat{G}|v + u\rangle$ to find the real part of $\langle v|\hat{G}|u\rangle$.

III. RESULTS AND DISCUSSION

In this section, we present and discuss binding energies and optical response of magnetoexcitons for a range of CNT and GNR geometries. All results have been obtained using $t = -3.0$ eV for the hopping integral and $s = 0.1$ for the overlap in the TB model. The spectra are normalized by a factor $\sigma_0 = e^2/d\hbar$ and convoluted with a Lorentzian line-shape function with a broadening of 0.08 eV. Convergence of the Lanczos-Haydock routine was obtained after 2000 iterations. The screening of the Coulomb matrix elements is set to $\epsilon = 3.5$, corresponding to CNTs in an aqueous solution [9]. For the exchange term, we find that a value of $\epsilon_{exc} = 2.5$ is appropriate, similarly to what was used in Ref. [44]. As our primary interest is a qualitative description of the effect of an external magnetic field on the excitonic response, we have used the same screening for the GNR calculations. So far, experimental absorption spectra for AGNRs are only available for AGNRs deposited on some type of metal [51,52]. Metal substrates strongly screen the Coulomb interaction and, hence, suppress the excitonic effects significantly.

We begin our presentation of the results by focusing on the real part of the diagonal optical conductivity elements σ_{zz} and σ_{yy}, denoting the parallel-polarized and cross-polarized absorption, respectively. The first and second column in Fig. 2 show the absorption spectra for (8,0) and (5,0) CNTs, respectively. In the considered photon energy range, there are two dominant peaks in the parallel-polarized exciton absorption of CNTs in the absence of magnetic fields. The peaks correspond to the first and second subband transitions and are typically denoted E_{11} and E_{22}. These spectra show the same features as spectra obtained using more advanced *ab initio* methods [42].

When the magnetic field becomes sufficiently strong, the Ajiki-Ando (AA) [18,19] splitting of the excitonic peaks in the σ_{zz} spectra can be observed. Without Coulomb effects (the dashed lines in Fig. 2), the splitting of the absorption peaks is caused by a field-assisted lifting of the twofold degenerate valence and conduction bands. Coulomb effects, i.e., excitons, lift the degeneracy partially and result in three exciton states: two nondegenerate (one dark and one bright) and a dark state, which is twofold degenerate [45]. The zero-field energy difference between the nondegenerate bright and dark exciton states is denoted Δ_{bd}. The observed splitting of the exciton absorption peak is then caused by the magnetic field brightening the nondegenerate dark exciton state and increasing the energy separation. The energy difference Δ_{bd} was reported in Refs. [19,43] to be proportional to $1/d_t^2$, where d_t is the CNT diameter. Similarly, both the field-dependent
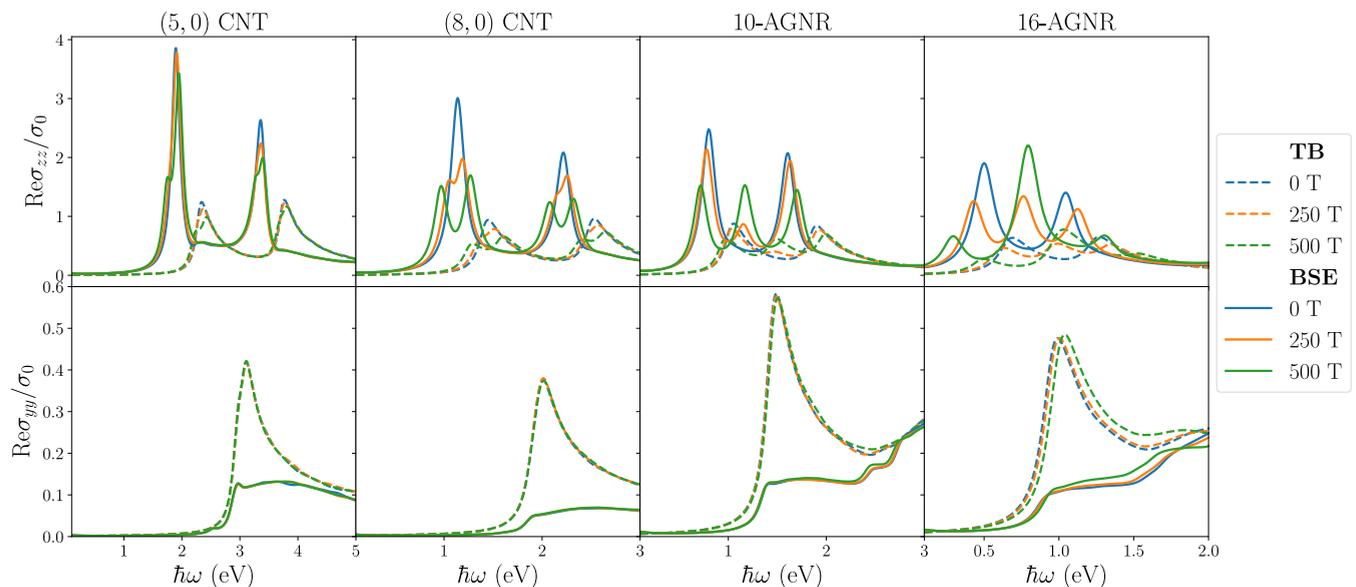
FIG. 2. Real part of the independent-particle (dashed lines) and excitonic (solid lines) diagonal conductivities σ_{zz} and σ_{yy} of (5,0) and (8,0) CNTs, and 10- and 16-AGNRs. The colors of the spectra correspond to the same magnetic field strengths in all plots. For the CNTs, the magnetic field is oriented in the parallel direction, while for GNRs it is oriented in the perpendicular direction.

increase in the energy splitting and the field-dependent change in oscillator strength of the bright and dark excitons depend on the CNT diameter [18,19]. The field-dependent increase in the energy splitting is proportional to d_t, while the changes in oscillator strength of the bright and dark excitons are dampened when Δ_{bd} is increasing[18]. Consequently, the observed splitting is not as clear for the (5,0) CNTs as for the (8,0) CNTs. For experimental observation of the AA splitting, one would need to use either large-diameter CNTs [20–22] or very strong fields [26], as illustrated here. The splitting we observe in the BSE results is comparable to what was reported in Refs. [18] and [19] using the $\mathbf{k} \cdot \mathbf{p}$ model, and what was observed experimentally for (6,5) CNTs in Ref. [26]. The AA splitting is only observed in parallel fields. The diagonal conductivities of CNTs in the presence of a perpendicular field do not show any significant change in fields up to 500 T and are therefore not shown.

Turning now to the diagonal conductivity tensor elements of AGNRs in perpendicular fields, the parallel- and cross-polarized absorption spectra are shown in the third and the fourth column of Fig. 2. The unperturbed spectra show two dominant exciton peaks similar to what was obtained using *ab initio* methods [7,12]. We reuse notation and denote the peaks by E_{11} and E_{22}. As the magnetic field strength is increased, the E_{11} peak is shifted to lower energies, and the shift of the peak is accompanied by a decrease in oscillator strength. Similarly, the E_{22} peak is shifted to higher energies and the oscillator strength of that peak is also decreased. Simultaneously, a new peak between the E_{11} and E_{22} peaks emerges for strong magnetic fields. We also observe that the effect is stronger for the wider AGNR, which is caused by the increased magnetic flux through the wider unit cell. Since there exists no experimental results regarding the optical response of magnetoexcitons in AGNRs yet, we cannot validate these changes in the spectra. But we expect that if AGNRs could be deposited on a nonmetallic material and aligned, the

change in the absorption spectrum could be measured in an experimental setup similar to that described in Ref. [26]. A common feature of both CNTs and AGNRs is that the effect of the magnetic field on the cross-polarized absorption is negligible and only causes small changes in the spectra. In addition, the inclusion of electron-hole interaction effects dampens the cross-polarized absorption due to strong depolarization [53].

The changes in the parallel-polarized absorption spectra are further elucidated in Fig. 3, which shows the smallest eigenvalues of the BSE for (8,0) CNTs and 10-AGNRs. The line color illustrates the optical intensity (oscillator strength) of the state associated with the eigenvalue. Figure 3(a) shows the lowest eigenvalues as a function of field strength for (8,0) CNTs in a parallel field. When there is no magnetic field, all but two of the exciton states are degenerate and only a single state is optically active. But, as the field strength is increased, the energies are altered and one of the dark excitons becomes optically active. This is what we observed as the splitting of the absorption peaks in Fig. 2. The field also lifts the degeneracy of the exciton states, and some eigenvalues are raised above the band-gap energy. We also see that the band gap of CNTs is affected by the external magnetic field and, e.g., in the case of (8,0) CNTs it decreases linearly. Whether the band gap increases or decreases with magnetic field depends on the family of CNTs considered [54]. Our results show a value of $\Delta_{bd} \approx 41$ meV at $B = 0$ T and a linear increase at high fields with a slope of approximately 0.54 meV/T. Comparing our results to the experimental results in Refs. [20–26], we see a larger value of Δ_{bd} and a smaller field-dependent increase in the splitting. As mentioned, this is due to the smaller diameter of the CNTs under consideration in this paper. If we compare to (6,5) CNTs and use the $1/d_t^2$ and d_t scaling on our results, we find $\Delta_{bd} \approx 28$ meV and a linear increase in the splitting of 0.65 meV/T at high fields. These values agree reasonably with experimental values [20–26]. Figure 3(b) shows the eigenvalues for 10-AGNR in
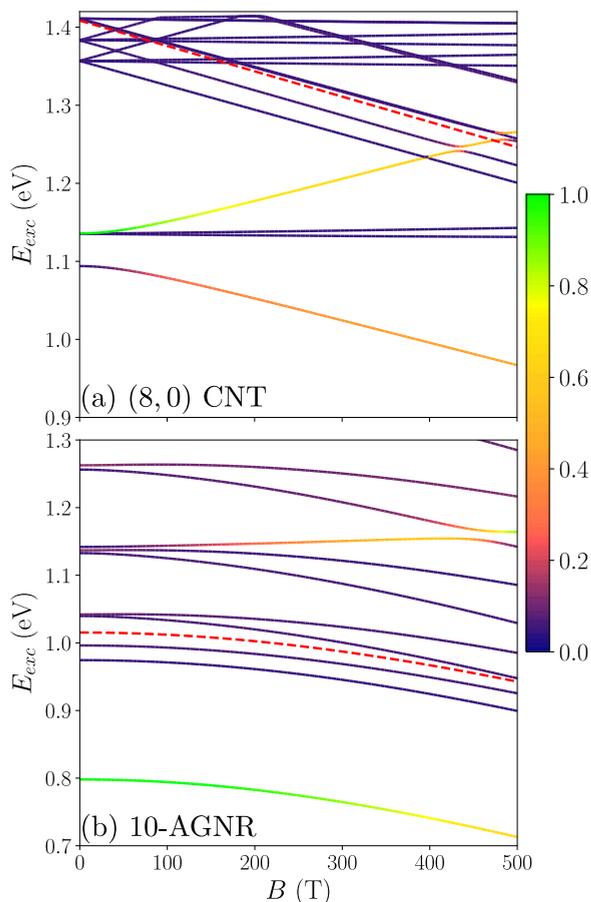
FIG. 3. Exciton energies as a function of magnetic field strength. The color of the lines in both plots corresponds to the relative optical intensity in the z direction, and the dashed red line is the band-gap energy. (a) Exciton energies of an (8,0) CNT in a parallel field. (b) Exciton energies of a 10-AGNR in a perpendicular field.

a perpendicular field. When the magnetic field strength is increased, the state associated with the E_{11} transition decreases in oscillator strength. Simultaneously, the oscillator strength of a state above the gap (at about 1.14 eV) is increased. Similar to what was observed for CNTs, the band gap of AGNRs is also altered by the magnetic field but not in a linear manner.

We now consider the Faraday rotation and Hall conductivities. In Figs. 4 and 5, the off-diagonal conductivities of CNTs and AGNRs, respectively, are shown. Generally, the off-diagonal optical conductivities are identically zero if there is no magnetic field to break time-reversal symmetry. Additionally, the electron-hole symmetry must be broken as clarified in Ref. [27], which is why a small overlap was included in the TB model. This could also have been achieved by including interactions beyond nearest neighbors in the TB model. Assuming that the complex refractive index in Eq. (9) is dominated by the surrounding media, the expression for the Faraday rotation of CNTs in an aqueous solution can be simplified to $\phi \approx l \mathrm{Re}\sigma_{xy}\rho/(2nc\epsilon_0)$. This holds, since $n \gg \kappa$ for water in the photon energy range where CNTs show absorption [55]. Consequently, the contribution of the CNTs to the Faraday rotation is proportional to the real part of the Hall conductivities. In Fig. 4, the real part of σ_{xy} for CNTs
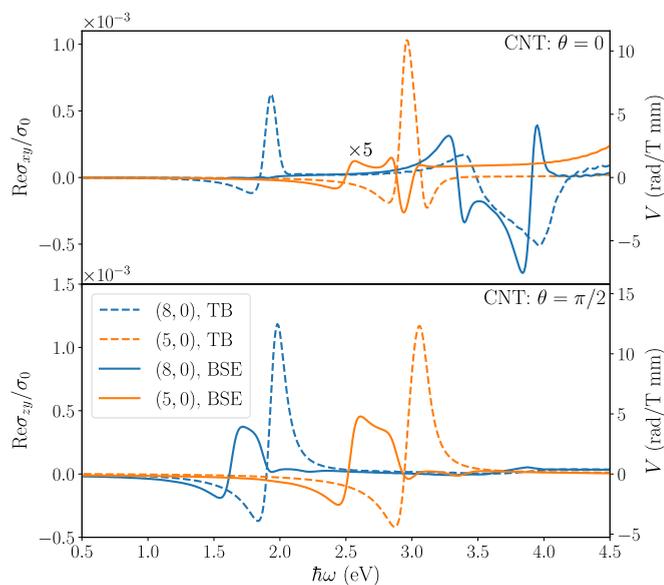

FIG. 4. Independent-particle and excitonic results for the dispersions of the Verdet constant and the real part of the off-diagonal conductivities of (5,0) and (8,0) CNTs for different directions of the magnetic field and $B = 10$ T.

in a parallel field and the real part of σ_{zy} for CNTs in a perpendicular field are shown, as well as the dispersion of the Verdet constant. The nonexcitonic results for $\mathrm{Re}\sigma_{xy}$ and the Verdet constant agree with Ref. [28]. But, in line with expectations, the excitonic effects significantly alter the Hall conductivities and the Faraday rotation. The plots clearly show that excitons must be included in a correct description of the Faraday rotation in CNTs. The other off-diagonal parts of the conductivity tensor are zero except for σ_{xy} in a perpendicular field, but this contribution is 3 orders of magnitude smaller than σ_{xy} in a parallel field. Thus, even for magnetic fields that
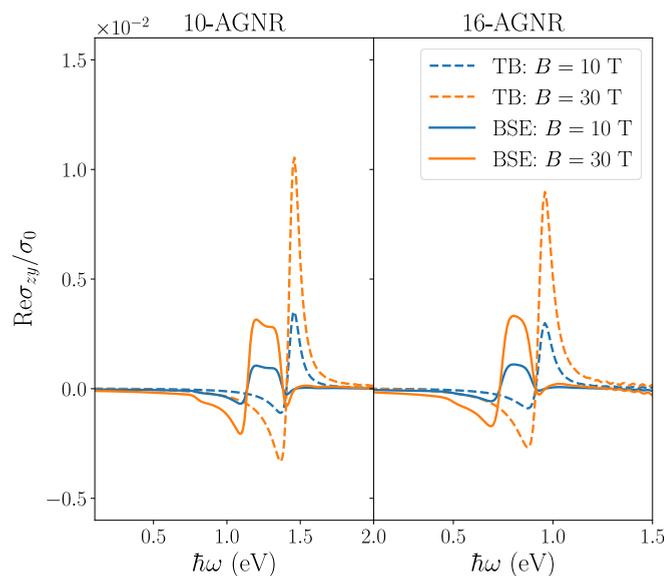

FIG. 5. Real part of the independent-particle and excitonic off-diagonal conductivities of 10- and 16-AGNRs in a perpendicular magnetic field.
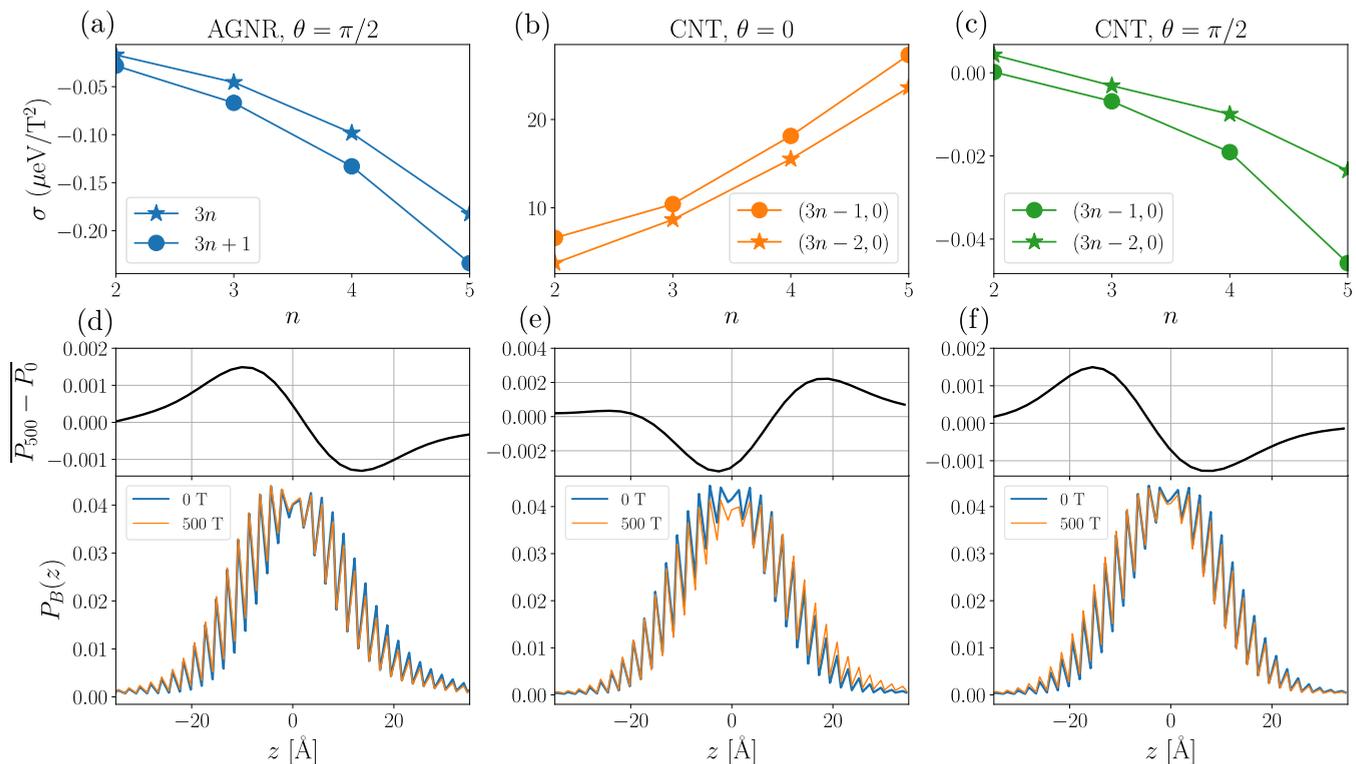
FIG. 6. (a–c) Diamagnetic coefficient of the low-energy bright exciton as a function of width or chiral indices for semiconducting families of (a) AGNRs in perpendicular fields and CNT in (b) parallel magnetic fields and (c) perpendicular magnetic field. (d–f) Exciton probability distribution with the hole located near the center of the unit cell for (d) 10-AGNR in a perpendicular field, (e) (8,0) CNT in a parallel field, and (f) (8,0) CNT in a perpendicular field. The top plots in (d–f) show the nearest-neighbor averaged change in the exciton probability distribution with magnetic field.

are not perfectly aligned with the axis of the CNT, the σ_{xy} conductivity is going to be dominated by the part related to the parallel field.

For AGNRs in a perpendicular field, the only finite Hall conductivity is σ_{zy}, which is shown in Fig. 5. The AGNR off-diagonal spectra underline the fact that the inclusion of excitonic effects is necessary for an accurate theoretical description of the optical response of AGNRs. For the magnetic field strengths considered in this paper, the off-diagonal conductivity scales linearly with field strength and the overall shape of the off-diagonal conductivity remains unchanged. This scaling holds true for both CNTs and AGNRs when the direction of the magnetic field is perpendicular to the directions of the off-diagonal element.

Finally, for the low-energy bright exciton we have evaluated both the diamagnetic coefficient and the exciton probability distribution. In real space, the exciton wave function can be written in the form $\Psi_{exc}(\mathbf{r}_e, \mathbf{r}_h)$. We fix the position of the hole $\mathbf{r}_h$ at an atom in the middle unit cell, and so the exciton probability distribution can be expressed as $P_B(z) = \sum |\Psi_{exc}(\mathbf{r}, \mathbf{r}_h)|^2$, where we sum over contributions with identical z coordinates and the subscript B denotes the magnetic field dependence. The diamagnetic shift ΔE_{dia} is the second-order change in exciton binding energy [56], i.e., $\Delta E_{\text{dia}} = \sigma B^2$, where σ is the diamagnetic coefficient. In Fig. 6, the diamagnetic coefficient for different semiconducting families of AGNRs and zigzag CNTs, the exciton probability distributions and the nearest-neighbor averaged change in exciton probability distributions

are shown. Figure 6(a) shows the diamagnetic coefficient of AGNRs in the presence of a perpendicular field. The negative coefficient $\sigma < 0$ shows that the binding energy of the ground-state exciton will increase as a function of field strength. In contrast, Fig. 6(b) shows that CNTs in a parallel magnetic field see a decrease in the binding energy for increasing field strength. The explanation for this observation is found in the geometries: The electron and hole in CNTs are restricted to the tube, and the parallel magnetic field increases the delocalization of the exciton wave function as illustrated by Fig. 6(e), where we see a decrease in the electron concentration around the hole. Consequently, the binding energy is decreased. On the other hand, the magnetic field increases the localization of the exciton wave function in AGNRs in a perpendicular field [see Fig. 6(d)] and the binding energy is increased. The increase in binding energy for AGNRs is in line with what is observed for monolayer materials [34]. Figure 6(c) shows the diamagnetic coefficient for CNTs in a perpendicular field. The results show that the shift changes from positive to negative as the tube radius increases. When the tube radius is large, the effect of the perpendicular magnetic field on the excitons will resemble that of AGNRs in a perpendicular field.

IV. SUMMARY

To summarize the work presented in this paper, we used a TB model and subsequently solved the BSE to study the optical properties of CNTs and AGNRs in the presence of a static

magnetic field. In both cases, pronounced excitonic effects are observed. We have shown that the optical absorption of AGNRs is significantly altered by a strong perpendicular field, while a strong parallel field alters the optical absorption of CNTs. For CNTs we see a field-dependent splitting of the exciton absorption peaks, caused by brightening of a dark exciton state, while a perpendicular field gives rise to a new absorption peak in AGNRs. We also calculated the different nonzero Hall conductivities, including excitonic effects for both CNTs and AGNRs. The calculations show that excitonic effects are essential for a correct evaluation of the off-diagonal conductivities and, hence, for the Faraday rotation. Finally, we have illustrated how the magnetic field changes the band gap, the exciton eigenvalues, and the localization of the exciton.

[1] D. V. Kosynkin, A. L. Higginbotham, A. Sinitskii, J. R. Lomeda, A. Dimiev, B. K. Price, and J. M. Tour, Nature (London) **458**, 872 (2009).

[2] L. Jiao, L. Zhang, X. Wang, G. Diankov, and H. Dai, Nature (London) **458**, 877 (2009).

[3] L. Liao, J. Bai, Y.-C. Lin, Y. Qu, Y. Huang, and X. Duan, Adv. Mater. **22**, 1941 (2010).

[4] J. Liu, A. Wright, C. Zhang, and Z. Ma, Appl. Phys. Lett. **93**, 041106 (2008).

[5] M. Terrones, A. R. Botello-Méndez, J. Campos-Delgado, F. López-Urías, Y. I. Vega-Cantú, F. J. Rodríguez-Macías, A. L. Elías, E. Munoz-Sandoval, A. G. Cano-Márquez, J.-C. Charlier *et al.*, Nano Today **5**, 351 (2010).

[6] J. M. Schnorr and T. M. Swager, Chem. Mater. **23**, 646 (2010).

[7] L. Yang, M. L. Cohen, and S. G. Louie, Nano Lett. **7**, 3112 (2007).

[8] T. G. Pedersen, Phys. Rev. B **67**, 073401 (2003).

[9] T. G. Pedersen, Carbon **42**, 1007 (2004).

[10] T. F. Rønnow, T. G. Pedersen, and H. D. Cornean, Phys. Lett. A **373**, 1478 (2009).

[11] B. Monozon and P. Schmelcher, Physica B **500**, 89 (2016).

[12] D. Prezzi, D. Varsano, A. Ruini, A. Marini, and E. Molinari, Phys. Rev. B **77**, 041404 (2008).

[13] J. A. Alexander-Webber, C. Faugeras, P. Kossacki, M. Potemski, X. Wang, H. D. Kim, S. D. Stranks, R. A. Taylor, and R. J. Nicholas, Nano Lett. **14**, 5194 (2014).

[14] A. V. Stier, N. P. Wilson, G. Clark, X. Xu, and S. A. Crooker, Nano Lett. **16**, 7054 (2016).

[15] B. A. Gregg, J. Phys. Chem. B **107**, 4688 (2003).

[16] J. Kalinowski, M. Cocchi, D. Virgili, P. Di Marco, and V. Fattori, Chem. Phys. Lett. **380**, 710 (2003).

[17] H. Ajiki and T. Ando, Physica B **201**, 349 (1994).

[18] T. Ando, J. Phys. Soc. Jpn. **73**, 3351 (2004).

[19] T. Ando, J. Phys. Soc. Jpn. **75**, 024707 (2006).

[20] S. Zaric, G. N. Ostojic, J. Kono, J. Shaver, V. C. Moore, M. S. Strano, R. H. Hauge, R. E. Smalley, and X. Wei, Science **304**, 1129 (2004).

[21] J. Shaver, J. Kono, O. Portugall, V. Krstić, G. L. Rikken, Y. Miyauchi, S. Maruyama, and V. Perebeinos, Nano Lett. **7**, 1851 (2007).

[22] R. Matsunaga, K. Matsuda, and Y. Kanemitsu, Phys. Rev. Lett. **101**, 147404 (2008).

[23] S. Takeyama, H. Suzuki, H. Yokoi, Y. Murakami, and S. Maruyama, Phys. Rev. B **83**, 235405 (2011).

[24] W. Zhou, T. Sasaki, D. Nakamura, H. Liu, H. Kataura, and S. Takeyama, Phys. Rev. B **87**, 241406 (2013).

[25] W. Zhou, T. Sasaki, D. Nakamura, H. Saito, H. Liu, H. Kataura, and S. Takeyama, Appl. Phys. Lett. **103**, 021117 (2013).

[26] D. Nakamura, T. Sasaki, W. Zhou, H. Liu, H. Kataura, and S. Takeyama, Phys. Rev. B **91**, 235427 (2015).

[27] T. G. Pedersen, Phys. Rev. B **68**, 245104 (2003).

[28] A. Zarifi and T. G. Pedersen, Phys. Rev. B **77**, 085409 (2008).

[29] L. Sun, S. Jiang, and J. Marciante, Opt. Express **18**, 5407 (2010).

[30] M. A. Schmidt, L. Wondraczek, H. W. Lee, N. Granzow, N. Da, and P. S. J. Russell, Adv. Mater. **23**, 2681 (2011).

[31] M. Tymchenko, A. Y. Nikitin, and L. Martin-Moreno, ACS Nano **7**, 9780 (2013).

[32] C. Ritter, S. S. Makler, and A. Latgé, Phys. Rev. B **77**, 195443 (2008).

[33] Y. Huang, C. Chang, and M.-F. Lin, Nanotechnology **18**, 495401 (2007).

[34] A. V. Stier, K. M. McCreary, B. T. Jonker, J. Kono, and S. A. Crooker, Nat. Commun. **7**, 10643 (2016).

[35] A. Mitioglu, P. Plochocka, A. Granados del Aguila, G. Christianen, G. Deligeorgis, S. Anghel, L. Kulyuk, and D. Maude, Nano Lett. **15**, 4387 (2015).

[36] A. A. Mitioglu, K. Galkowski, A. Surrente, L. Klopotowski, D. Dumcenco, A. Kis, D. K. Maude, and P. Plochocka, Phys. Rev. B **93**, 165412 (2016).

[37] G. Plechinger, P. Nagler, A. Arora, A. Granados del Aguila, M. V. Ballottin, T. Frank, P. Steinleitner, M. Gmitra, J. Fabian, P. C. Christianen *et al.*, Nano Lett. **16**, 7899 (2016).

[38] A. V. Stier, N. P. Wilson, K. A. Velizhanin, J. Kono, X. Xu, and S. A. Crooker, Phys. Rev. Lett. **120**, 057405 (2017).

[39] R. Saito, G. Dresselhaus, and M. S. Dresselhaus, *Physical Properties of Carbon Nanotubes* (World Scientific, Singapore, 1998).

[40] S. Reich, J. Maultzsch, C. Thomsen, and P. Ordejon, Phys. Rev. B **66**, 035412 (2002).

[41] W. Kohn, Phys. Rev. **115**, 1460 (1959).

[42] C. D. Spataru, S. Ismail-Beigi, L. X. Benedict, and S. G. Louie, Phys. Rev. Lett. **92**, 077402 (2004).

[43] C. D. Spataru, S. Ismail-Beigi, R. B. Capaz, and S. G. Louie, Phys. Rev. Lett. **95**, 247402 (2005).

[44] T. G. Pedersen, Phys. Rev. B **69**, 075207 (2004).

[45] V. Perebeinos, J. Tersoff, and P. Avouris, Phys. Rev. Lett. **92**, 257402 (2004).

[46] L. X. Benedict, Phys. Rev. B **66**, 193105 (2002).

[47] M. L. Trolle, G. Seifert, and T. G. Pedersen, Phys. Rev. B **89**, 235410 (2014).

[48] T. G. Pedersen and K. Pedersen, Phys. Rev. B **79**, 035422 (2009).

[49] I. Crassee, J. Levallois, A. L. Walter, M. Ostler, A. Bostwick, E. Rotenberg, T. Seyller, D. Van Der Marel, and A. B. Kuzmenko, Nat. Phys. **7**, 48 (2011).

[50] R. Haydock, Comput. Phys. Commun. **20**, 11 (1980).

[51] S. Linden, D. Zhong, A. Timmer, N. Aghdassi, J. Franke, H. Zhang, X. Feng, K. Müllen, H. Fuchs, L. Chi *et al.*, Phys. Rev. Lett. **108**, 216801 (2012).

[52] R. Denk, M. Hohage, P. Zeppenfeld, J. Cai, C. A. Pignedoli, H. Söde, R. Fasel, X. Feng, K. Müllen, S. Wang *et al.*, Nat. Commun. **5**, 5253 (2014).

[53] S. Uryu and T. Ando, Phys. Rev. B **74**, 155411 (2006).

[54] J. P. Lu, Phys. Rev. Lett. **74**, 1123 (1995).

[55] G. M. Hale and M. R. Querry, Appl. Opt. **12**, 555 (1973).

[56] S. N. Walck and T. L. Reinecke, Phys. Rev. B **57**, 9088 (1998).